Distortion Analysis in the Manufacturing of Cold-Drawn and Induction-Hardened Components

THOMAS GEORG KARL HIRSCH, ALEXANDRE DA SILVA ROCHA, and RAFAEL MENEZES NUNES

In this investigation, a design of experiments analysis of distortion for a typical manufacturing process involving pre-straightening, cold drawing, and induction hardening of AISI 1045 cylindrical steel bars was carried out. A careful characterization of the material, including residual stress states and geometrical changes, was done for the different manufacturing steps. In order to identify effects and correlations on distortion behavior, the investigated variables included the batch influence, the combined drawing process itself with two different drawing angles and two different polishing and straightening (P.S.) angles, a stress relief treatment which was applied to a part of the samples, and finally induction hardening with two different surface hardening depths. Main and statistically significant effects on the distortion of the induction-hardened samples were found to be in this order: first, the interaction between the drawing angle and batch, then the interaction between drawing angles, and finally drawing angle and induction hardened layer. It was also found that the distortion potentials are transmitted from the drawing process to further manufacturing steps and, consequently, from one production site to the next.

DOI: 10.1007/s11661-013-1952-z

I. INTRODUCTION

MANUFACTURING processes of metals in general consist of materials solidification processes, metal-forming processes, more than one straightening process, and machining and heat treatment processes.[1,2] Machining and final straightening are then necessary to guarantee the required shape and dimensions of machine parts. Cold forming significantly changes a material's properties, and cold-formed automotive parts need a surface heat treatment or should be through hardened to fulfill strength requirements. Changes in processing parameters of material properties for one production step can consequently result in problems in the next, one of the following, or in the last manufacturing step. Components manufactured in this way show a broad band of distortions, which have to be removed by additional expensive machining operations.[3,4]

It is well known that distortion of components is connected to the whole manufacturing history and depends on[5] (a) the components' geometry; (b) the chemical composition and local variations; (c) the mechanical history of the components; (d) on local time–temperature sequences during manufacturing; (e) on the (local) microstructure and phase transformations at temperature; and (f) on the generation and relaxation of stresses/residual stresses.

The manufacturing chain in this investigation starts with an AISI 1045 wire rod with a nominal diameter of 21.4 mm which was hot rolled and stored in coils and ends with induction-hardened small bars of 200 mm length. First, the wire rod is pre-straightened and shot blasted; then, in the same manufacturing line, it is cold drawn; and finally an additional polishing and straightening (P.S.) step is carried out after drawing to obtain straight bars of 6 m length.[6,7] After that, to simulate the manufacturing of shafts and to evaluate the distortion, the bars are cut, a stress relief treatment can be optionally added, and finally the induction hardening of a small surface layer is carried out.

A design of experiments (DoE) plan with main affecting parameters as the drawing process itself with two different drawing angles, a stress relief treatment which was applied to one part of the samples, and finally an induction heat treatment with two different surface hardening depths is used to identify effects and correlations on the final distortion after induction hardening as a result of the whole manufacturing chain.

II. MATERIALS AND MICROSTRUCTURES

The material was an AISI 1045 steel with the chemical composition given in Table I. One example of local chemical compositions and microstructures is presented in Figure 1. The bars can be characterized by a distribution of segregations, *e.g.*, by a central positive segregation and as proved by microprobe analysis some inhomogeneous distribution of carbon. Minimum carbon contents of 0.3 Mass pct and maximum values of

THOMAS GEORG KARL HIRSCH, Research Director, is with the Stiftung Institut für Werkstofftechnik, Bremen, Germany. ALEXANDRE DA SILVA ROCHA, Professor, is with the Centro de Tecnologia, Universidade Federal do Rio Grande do Sul, Porto Alegre, Brazil. RAFAEL MENEZES NUNES, Postdoctoral Researcher, is with the LAMEF, Universidade Federal do Rio Grande do Sul, Porto Alegre, Brazil. Contact e-mail: Rafael.nunes@ufrgs.br
Manuscript submitted February 15, 2013.
Article published online August 28, 2013

Table I. Chemical Composition of the Investigated AISI 1045 Steel

Element	C	Si	Mn	P	S	Cr	Mo	Ni	Cu	Nb
Mass pct	0.43	0.24	0.79	0.03	0.02	0.13	0.03	0.08	0.1	<0.01

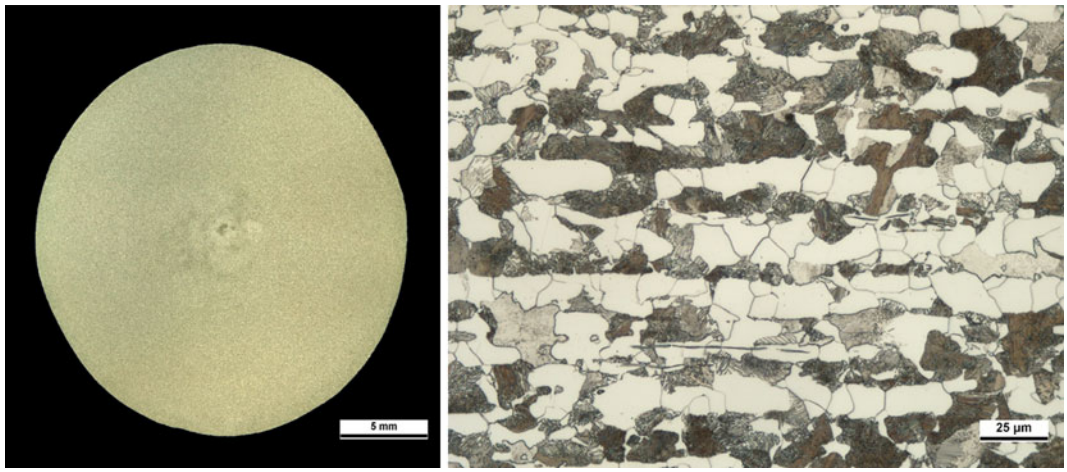

Fig. 1—Macro image of a radial cross section (left), axial microstructure of the material (right).

0.6 Mass pct were analyzed in radial cross sections by quantitative microprobe analysis. Consequently, the microstructure in Figure 1 is a banded structure with higher and lower amounts of Pearlite grains. Statistical evaluation of microstructures resulted in a mean ASTM grain size between 10 and 11. Grain size distributions varied depending on the location of specimens prepared for the microstructural analysis. The chemical and microstructural analysis typifies the material as typical industrially processed medium carbon steel.

After the cold drawing and final straightening, samples of diameter 20.25 mm and length 200 mm were manufactured to analyze the distortion in the manufacturing chain of the investigated combined cold drawing process (Figure 2).

Induction hardening was done vertically with a multi-frequency machine from the company EFD in Germany (type SINAC 200/300 FMC®). An inductor of diameter 22 mm was firstly placed at the bottom of the bar and then moved upward with feed rates between 2 and 1.4 m/min at a frequency of 238 kHz to result in the desired surface hardening depth. Quenching nozzles were placed underneath the inductor and fed a 12 pct concentration of Aquatensid® polyalkylene glycol (PAG)-based solution. After induction hardening, the metallographical analysis showed fine martensite in the near surface layers. Some isolated ferrite could be identified up to a 10-μm distance from the surface due to some decarburizing. Retained austenite was present with an amount of 5 to 8 vol pct until 50 pct of the surface hardening depth due to the inhomogeneous distribution of ferrite and pearlite lines (see Figure 1). Surface hardening depths at 80 pct of minimum required hardness were 0.63 and 1.1 mm.

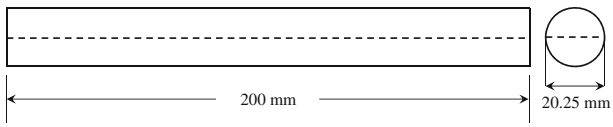

Fig. 2—Size and shape of cold-drawn bars for the dimensional analysis, units in mm.

III. EXPERIMENTAL DETAILS

Investigations of distortion potential carriers and distortion itself require a high amount of different analysis methods. These will be described briefly. Figure 3 presents the investigated manufacturing process starting with horizontal coils. The initial mean diameter of the hot-rolled wire is 21.4 mm. The diameter of the wire, however, varies along its length and exhibits diameter variations from 20.31 to 21.76 mm. This wire is vertically and horizontally straightened, shot blasted, and then drawn with two different drawing angles of 15 and 20 deg ($\alpha^1 = 7.5$ and 10 deg) with final dimensions of 20.25 mm. New polished tools were used for each drawing experiment. From this reduction in diameter, the area reduction is 12.3 pct. After drawing, the wire is shear cut into 6-meter bars. A combined P.S. process is applied to these 6-meter bars; this process is further addressed as P.S. From these bars, the samples were cut into pieces of 200 mm length by a simple sawing machine. After this procedure and first 3D measurements of the geometry, a part of samples was stress relieved in a vacuum furnace with the help of a pressurized nitrogen atmosphere at temperatures of 773 K and 873 K (500 °C and 600 °C). Finally, induction hardening with two different surface hardening

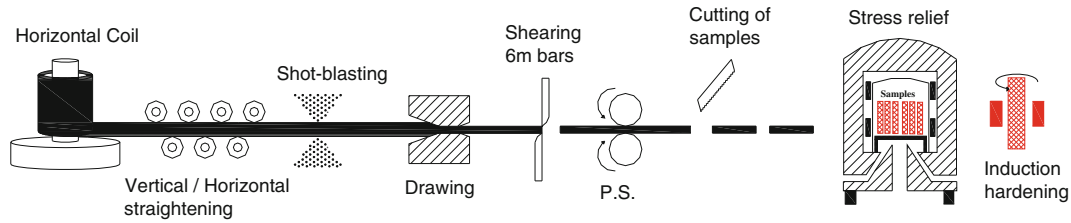

Fig. 3—The investigated manufacturing chain (P.S. is combined polishing and straightening).

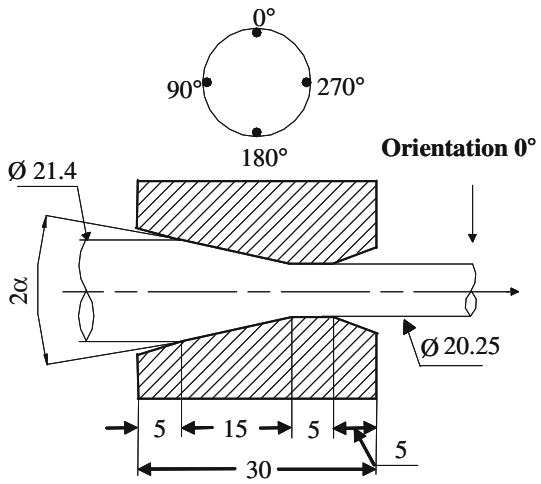

Fig. 4—Schematic view of the drawing process, orientation system, and tool dimensions (units in mm).

depths of 1.1 and 0.63 mm ended this manufacturing sequence. Marked peripheral angular positions around the bars were used as reference for any experimental and dimensional analysis. The "0 deg" position is a horizontal line on the uppermost position of the rods as they pass through the drawing tool and any further manufacturing step (see Figure 4).

The following DoE plan (Table II) was executed with 3 samples for each batch. Dimensional analyses after drawing, P.S. stress relief (SR), and induction hardening (IH) were carried out with a Zeiss® Contura G2 3-D machine and a Leitz® PMM 654 machine. Each cylinder was clamped in the central plane with the 0 deg line always pointing to the top of the cylinders. 12 circles of measurement were used to define the shape and size of the cylinders with 360 points each at 2, 8.5, 16, 25, 50, 70, 130, 150, 175, 184, 191.5, and 198 mm distance from one end of the sample. Each circle then was fitted with a best fit circle by a least squares method.[8,9] From these calculations, the center positions of each circle are known. The projection of these positions on an imaginary X–Y plane in the axial center of each bar creates a vector. The vector length is an expression for the curvature, and its orientation in the X–Y plane is the expression of the orientation of this curvature. The software "Minitab®" was used for the statistical evaluation of the DoE with a given statistical significance of 98 pct ($\alpha = 0.02$).

Residual stress X-ray diffraction (XRD) analysis used the conventional $\sin^2\psi$-method with conventional Bragg–Brentano Geometry. A Bruker®-AXS D8 system was employed using Vanadium filtered Cr-Kα radiation. A primary beam aperture of 2 mm diameter was selected for the local analysis along the length and around the periphery of the drawn cylinders. The {211}-lattice planes of α-iron were measured and any further measurement procedure and evaluation followed procedures which are described in.[10] The 1045 steel contains 6.7 vol pct of Cementite (Fe_3C). The literature results of residual stresses in Cementite after drawing processes, however, point to very high tensile residual stresses in the axial direction with values of more than 2000 MPa.[11–13]

Table II. Design of Experiments Plan: +1 is 20 deg Drawing Angle, 16 deg P.S. Angle, 873 K (600 °C), and 0.63-mm Surface Hardening Depth; −1 is 15 deg Drawing Angle, 18 deg P.S. Angle, No Stress Relief, and 1.1-mm Surface Hardening Depth

A (Batch)	B (Draw Angle)	C (P.S. Angle)	D (Stress Relief)	E (SHD in IH)
−1	1	−1	−1	1
−1	−1	1	−1	−1
1	−1	1	−1	1
1	1	1	−1	−1
−1	1	1	1	1
−1	1	−1	1	1
1	−1	−1	1	−1
1	1	−1	1	1
−1	1	−1	1	−1
1	1	−1	1	−1
−1	−1	1	−1	1
1	1	−1	−1	1
−1	1	1	1	−1
−1	1	−1	−1	−1
1	−1	1	1	−1
1	−1	1	−1	−1
−1	1	1	−1	1
−1	−1	1	1	−1
1	−1	−1	−1	1
1	1	1	−1	1
1	−1	−1	1	1
1	1	1	1	−1
−1	−1	−1	−1	−1
−1	−1	−1	1	1
1	−1	−1	−1	−1
−1	−1	−1	1	−1
1	1	1	1	1
1	1	−1	−1	−1
−1	1	1	−1	−1
−1	−1	−1	−1	1
1	−1	1	1	1
−1	−1	1	1	1

Table III. Phase Stresses in Cementite After Different Manufacturing Steps Weighted Over a 60-μm Surface Layer

Manufacturing Parameter	Drawn 20 deg	Drawn 15 deg	Drawing 20 deg, Polishing/Straightening 16 deg	Drawing 20 deg, Polishing/Straightening 18 deg
Phase Stresses in Fe_3C (MPa)	2620	2180	−56	370

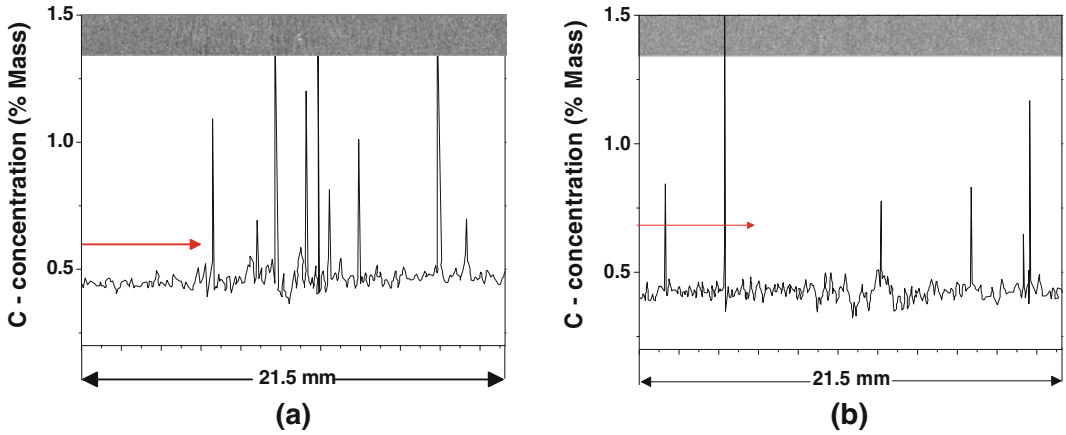

Fig. 5—Quantitative chemical composition by microprobe analysis (C-Kα with 20-μm beam at 15 kV, 1000 × 200 points) along one diametrical line of in the cross sections for the as-delivered state of material in batch +1 (*a*) and batch −1 (*b*). The arrows in both picture points to a similar distance from one end of the cross section.

Measurements of the authors at the synchrotron radiation facility BESSY II in Berlin pointed to similar values.[14] The following Table III gives a short overview and additionally provides information about the following manufacturing steps. The surface residual stresses in the Cementite decrease drastically after the P.S. manufacturing step. Finally, for the AISI 1045 material, the calculation of micro-residual stresses in the two phases Ferrite and Cementite, the calculation of macro-residual stresses, and the consideration of a macroscopic three-dimensional stress state in surface layers[12] of the different manufacturing steps gave a small difference to measured residual stresses. Taking into account that the differences are not highly significant and the impossibility of data acquisition for all different manufacturing steps over each cross section for ferrite and additionally cementite, in further results only the data of phase residual stress in ferrite will be communicated.

Measurements of residual stresses concentrated on axial residual stresses as samples show a clear bending state of distortion. Measurements of the hoop direction, however, proved a reasonable symmetry of the residual stress state, almost equal values in the axial and hoop direction. Neutron diffraction residual stress measurements were performed at the Helmholtz-Zentrum-Berlin in Germany on beam line E3 of the BER II reactor. Further details about the equipment and the beam line can be found in.[15] Measurement procedures and sequence of calculating force equilibriums of macro-residual stresses and iteratively corrected d_0 values for the Neutron diffraction residual stress determination followed procedures described in.[10,16]

Local strength analysis was done by microhardness testing. Radial cross sections of drawn bars were analyzed with a couple of 316 individual $HV_{0.1}$ hardness indentations. To overcome problems with scatter, partial means of hardness were calculated in the following way: For each measured diametrical line, means are presented for the first 5 mm (0 to 5 mm), for the central 5 mm (7.5 to 12.5 mm), and for the last 5 mm (15.25 to 20.25 mm).

IV. RESULTS

A. *General Statement on Distortion Potential Carriers*

Distortion potential carriers will be described briefly. For distortion potential carrier "chemical composition and microstructure," some local chemical and microstructural differences have already been presented in Figure 1. Figure 5 quantifies local chemical composition along one diameter of an as-delivered hot-rolled wire. The black horizontal bar is an image of the microprobe area with a 20-μm beam (15 kV). The C-Kα line was recorded for 1000 points along the diameter and for 200 points perpendicular to it. An integration over these vertical points resulted in the local carbon concentration. As expected, the mean carbon concentration equals the value from Table I. In segregated locations, however, minimum values of 0.3 mass pct and maximum values of 0.6 to 0.7 mass pct change time-transformation diagrams and contribute to local different transformation behavior during hot rolling and induction hardening. Comparing two different batches of material with nominal compositions as given in Table I, a positive segregation at arrow position for batch +1 can be seen in Figure 5(a) and a negative segregation at the same position for batch −1 in Figure 5(b). Consequently, an effect on distortion behavior and a somewhat different behavior from one sample to the next can be expected for the two different batches in consideration.

B. *Distortion Potential Carriers Ahead of the Drawing Process*

The first manufacturing step after uncoiling is pre-straightening. Shot blasting will remove hot rolling scale and/or iron oxides from hot rolling and storage of coils. Consequently, residual stresses in the bar cannot be zero ahead of drawing, and compressive residual stresses are expected in a thin surface layer from shot blasting. Figure 6(a) gives an image of axial residual stresses in pre-straightened bars along the length of the bar. To avoid any effect from shot blasting, these measurements have been taken at 1.8-mm surface distance and so far were able to separate effects from the pre-straightening and shot blasting. Depth corrections of residual stresses for layer removal of cylindrical bodies have been applied.[17] Residual stresses vary along the length of the bar. For 135-, 180-, and 225 deg angular positions, positive values of residual stresses occur, whereas for example at 315, 0, 45, and 90 deg, compressive residual stresses were measured. It is so far obvious that the wire after pre-straightening shows a pronounced local state of bending residual stresses in one cross section. Variation along the length of the bars is also obvious. In Figure 6(b), residual stresses throughout the cross section of a pre-straightened sample are presented from Neutron diffraction measurements. The radial distance has been normalized to sample radius. It has been put to square for axial direction to show the equilibrium of forces. Squared radial values for the axial direction have partially been given a negative sign to gain a complete residual stress distribution along one diameter. Hoop equilibrium can be verified from the normalized radii as well. As the abscissa contains two different scales, the maximum tensile residual stresses occur apparently at different normalized radial positions. Low negative values at the center are observed, which are shifted to tensile values of 70 MPa for normalized distances of about 0.5 mm^2. Near surface axial and hoop residual stresses are shifted to compression as expected from shot blasting. Surface XRD analysis resulted in similar quantities if Neutron diffraction results are extrapolated to the surface. The open squares and triangles in Figure 6(b) result from XRD measurements and despite the different volume elements of the two stress analysis methods, a good correlation is present. Residual stresses are the consequence of locally different elastic–plastic deformations.

C. *Distortion Potential Carriers After Drawing and P.S.*

A local different mechanical history of drawn bars should contribute to distortion. For example, local inhomogeneities in strength after drawing should find their expressions in local microhardness variations. Figure 7 presents mean hardness values for different diametrical lines defined by the peripheral angles as presented in Figure 4. For drawing angle 20 deg, an increase can be found for 0 to 180 deg from the lowest hardness around the 0 deg position (0 to 5 mm) to the highest values at the 180 deg position, resulting in strength asymmetries. Surface layers after 15 deg drawing have higher hardness compared to the center. The 90 deg/270 deg line on Figure 7(a) differs from the 0 deg/180 deg orientation contributing again to an asymmetry around the periphery. The lower drawing angle gives more homogeneous distribution for the 90 deg/270 deg orientation with the lowest values in the center.

After the drawing process, symmetric residual stress distributions in a central plane are presented in Figure 8(a). The axial and hoop equilibrium of residual stresses is obvious. As expected, high tensile residual stresses of up to 450 MPa for the axial and hoop direction were observed in surface layers and compressive residual stresses of −450 MPa are present in the center. The radial residual stresses in the near surface layers are zero and show compressive values of up to −200 MPa in the center of the bar. However, radial residual stresses are calculated after force equilibrium for axial and hoop directions with the d_0 value then obtained.[10] Radial stresses are consequently the result of the force equilibrium calculation for axial and hoop

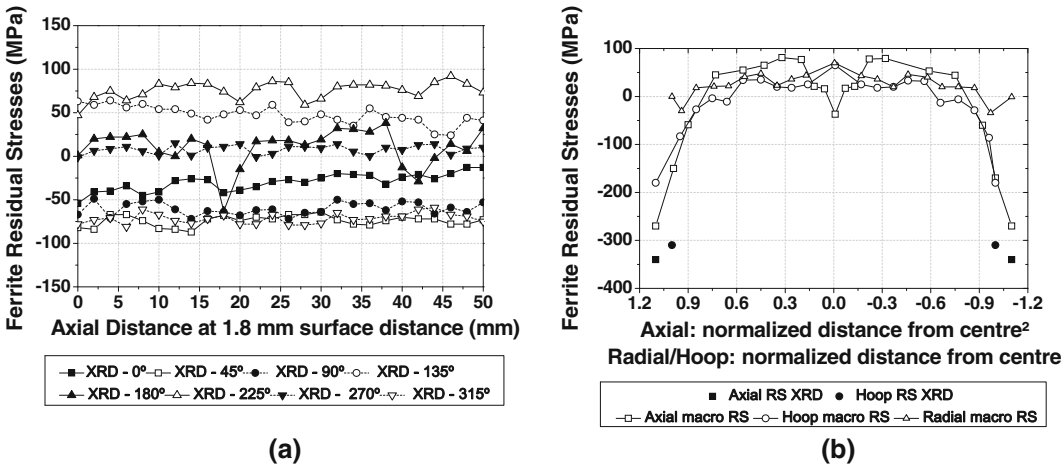

Fig. 6—Overview of residual stress fields (RS) in pre-straightened bars at surface distance of 1.8 mm (*a*) and axial and hoop, radial residual stresses as a function of r^2 (axial direction) and r (radial and hoop direction), respectively (*b*). Surface values were determined by X-ray diffraction (XRD) and values from cross sections by non-destructive neutron diffraction.

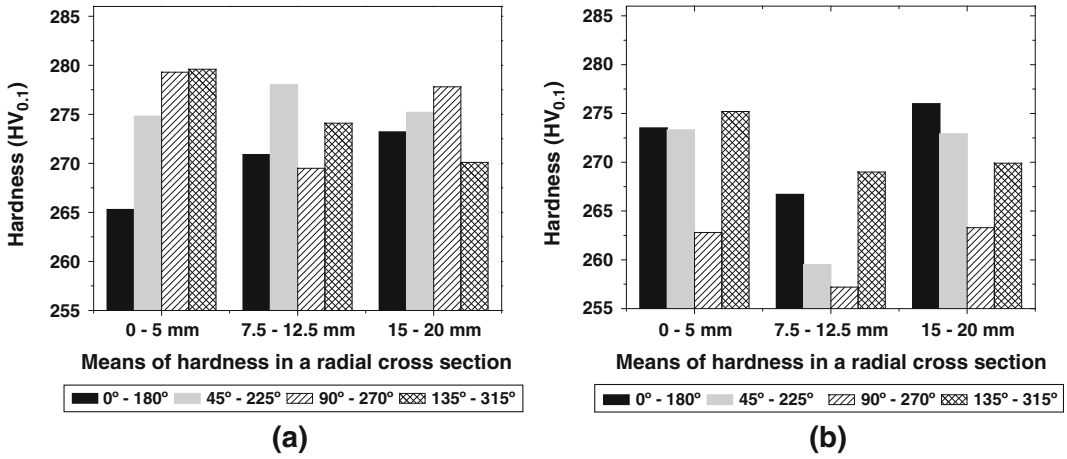

Fig. 7—Means of hardness in a radial cross section (*a*) drawing angle 20 deg, (*b*) drawing angle 15 deg.

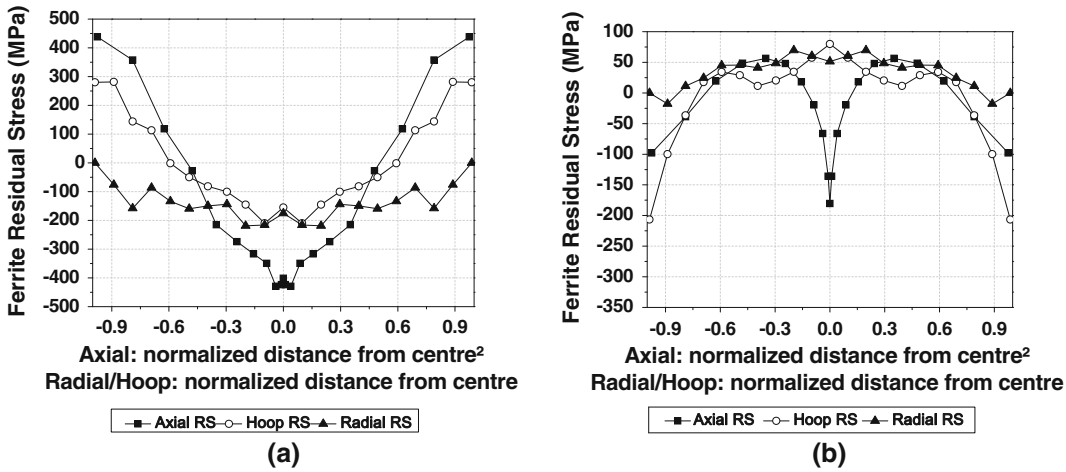

Fig. 8—Overview of residual stress distributions in drawn bars with drawing angle 20 deg (*a*) and in (*b*) straightened and polished bars (P.S.) with a cross roll angle of 16 deg. Axial and hoop, radial residual stresses as a function of r^2 (axial direction) and r (radial and hoop direction), respectively.

direction. The drawing angle of 15 deg gives similar distributions with values of maximum 50 MPa difference compared to the higher drawing angle concerning the variation of residual stresses along the surface, asymmetry around the surface, and distribution of residual stresses in the cross section.

Figure 8(b) shows residual stresses for the next manufacturing step. As expected, the P.S. process changes the residual stress state in the cross section completely. The high tensile residual stresses at the surface of drawn bars are shifted to compressive residual stresses and redistribution can be observed throughout the remaining cross section. Some tensile residual stresses, however, remain for the axial and hoop direction at 50 pct of the radius. In the center of the bar, axial residual stresses are still in compression, while hoop residual stresses are in tension. Radial residual stresses after the calculation for force equilibrium can be found to be about 50 MPa in tension which is in the order of precision to be reached by Neutron diffraction measurements.

D. *Distortion Potential Carriers in Induction-Hardened Bars*

Residual stress relief effects for AISI 1045 steel in different material states can be calculated according to equations given in.[18] Residual stresses at surface and after 50-μm layer removal proved to be near zero. It is so far obvious that drawing and P.S.-induced residual stresses could be relieved after stress relief.[18] Induction-hardened bars after stress relief consist of a surface-hardened layer with hardness depth profiles from Figure 9(a). Compressive residual stresses of −650 MPa occur in the surface-hardened layer and a strong gradient is present in the transition zone (see Figure 9(b)). Again, a symmetric distribution of residual stresses is presented to demonstrate the stress equilibrium. High tensile residual stresses after induction hardening were observed at the same surface distances, as tensile residual stresses have been left from the drawing and P.S. The residual stress state in the hardened layer is rotationally symmetric and similar

values occur for the axial and hoop direction. With increasing surface distance, residual compressive stresses decrease and are shifted to tensile residual stresses. These maximum tensile residual stresses of 400 MPa which are present at 80 pct of the radius occur just beneath the induction-hardened layer and exhibit similar magnitudes for hoop and axial direction at the same radial position. From other results, which are not presented here due to limited space, it is obvious that different drawing angles do not affect the residual stress distribution in the induction-hardened layer. The induction heat treatment and its parameters determine the surface hardening depth as well as the distribution of residual stresses and hardness. Within small experimental error, the distributions after different steps of manufacturing but similar induction hardening treatments match each other.

E. *Analysis of Distortion: Size and Shape Changes*

Figure 10 presents some detailed data of the dimensional analysis after each step of the manufacturing for two individual bars. Diameters are different after the drawing with 15 deg and with 20 deg (see black quadratic symbols in Figure 10). In either case, a stress relief treatment reduces the size (nominal diameter) and induction hardening increases diameters compared to the diameter of the originally drawn, polished, and straightened bars. Figure 11 summarizes the size changes of all investigated samples. To generate Figure 11, diameter changes after drawing and P.S., stress relief (SR), and induction hardening (IH) were calculated with a subtraction of a reference value of 20 mm, and changes of bars drawn with 20 deg are displayed against those drawn with 15 deg to obtain a 2-dimensional plot. With this procedure, differences between the different manufacturing parameters can be magnified. As known from any dimensional analysis, scatter of results is present in each manufacturing step. On the other hand, results can be grouped by circles and/or ellipses which include all individual results of one set of manufacturing parameters. Numbers indicate the angle of crossed rolls in polishing and straightening. For a given diameter change after drawing, drawing with 20 deg gives higher nominal diameters for the P.S. angle of 16 deg compared to those of 18 deg. Stress relief for the

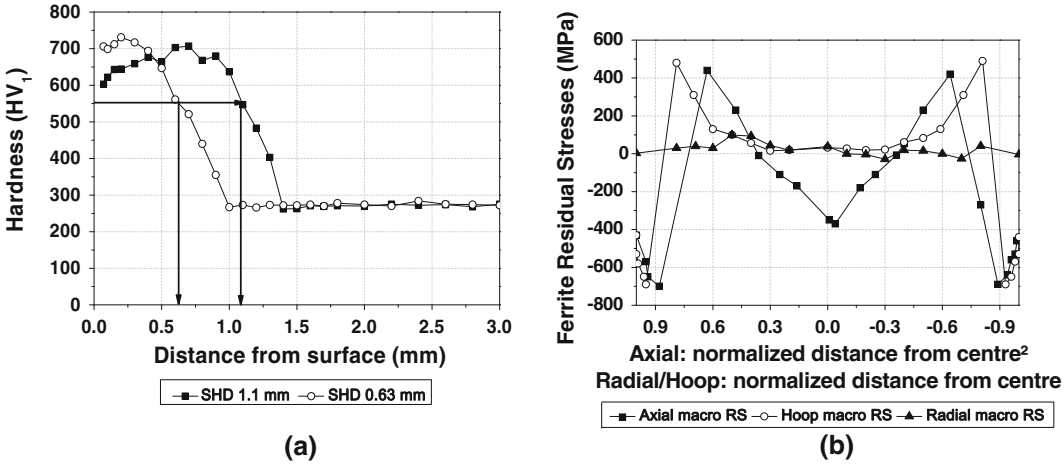

Fig. 9—Distribution of hardness (*a*) and residual stresses (RS) in an induction-hardened shaft (*b*) (SHD = 0.63 mm).

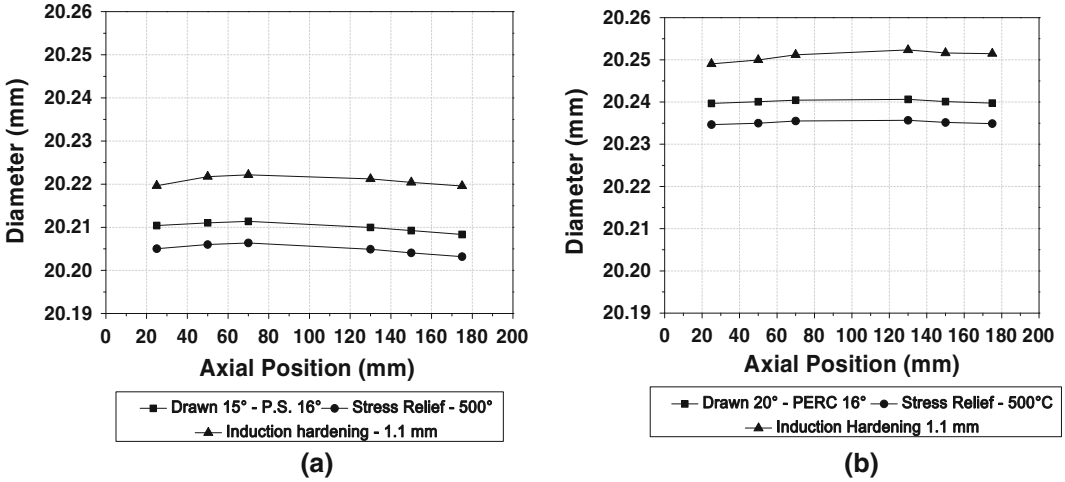

Fig. 10—Diameter and shape changes of two samples after drawing and P.S., stress relief, and induction hardening.

two temperatures of 773 K and 873 K (500 °C and 600 °C) is shifting the diameters of both groups with similar distances to lower diameters, and differences between the different angles 16 and 18 deg remain as seen from Figure 10. The mean nominal diameter decreases. The induction hardening then increases the size, and differences to the original drawing/P.S. process can be identified again. Samples without stress relief, however, for each set of manufacturing parameters show the highest diameter changes (triangles in the upper right direction in Figure 11).

Similarly, Figure 12 summarizes the value of the distortion vector (shape changes) plotted in the form of *x*- and *y*-coordinates of the distortion vector. As already mentioned in the experimental procedure, shape changes were characterized with a vector given by best fit circle center positions plotted on a fictitious central plane. Results were again grouped by circles: one for manufacturing parameters 15 deg drawing, 16 and 18 deg angle of rolls for the straightening and polishing, with stress relief and results of the two different induction hardening depths (dotted circle). The full circle describes results of the 20 deg drawing, 16 and 18 deg angle during the straightening and polishing, stress relief, and the two different induction hardening depths. Radii were determined by maximum values of *x*- and *y*-coordinates for each group. Obviously, the two main groups differ in size, and all data after manufacturing with a 20 deg drawing angle in general show higher deviations in *x*- and *y*-coordinates of distortion vectors. Different deviations can be verified additionally after straightening and polishing and the stress relief treatment indicating a different behavior at this step of manufacturing. Similar to the size behavior, samples that were not stress relieved show the highest distortion for the 15 deg and the 20 deg drawing at the end of the manufacturing (in the induction-hardened state).

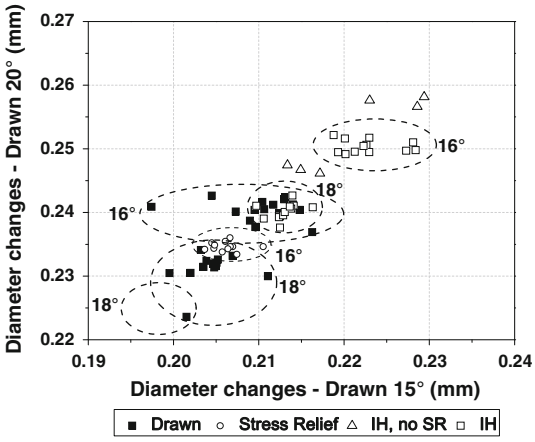

Fig. 11—Size changes after different manufacturing steps. Diameter changes after drawing and P.S. (numbers indicate the angles between polishing rolls), stress relief (SR), and induction hardening (IH) were calculated and changes of bars drawn with 20 deg drawing angle are displayed against those drawn with 15 deg to obtain a 2-dimensional plot.

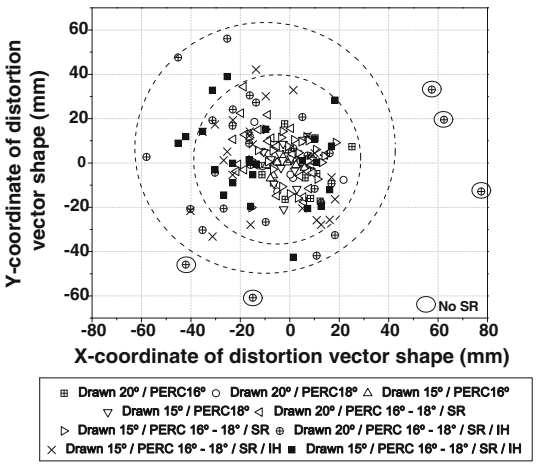

Fig. 12—Shape changes after different manufacturing steps plotted as *x*- and *y*-coordinates of the distortion vector.

Figures 11 and 12 give an indication of distortion effects due to different manufacturing steps. The statistical analysis of the DoE plan in Table II with a confidence level of $\alpha = 0.02$ (98 pct) finally identifies statistically significant manufacturing parameters for distortion after induction hardening due to the different manufacturing steps. Figures 13 and 14 give second- and third-order results for distortion. Minitab displays the absolute value of the standardized effects on the Pareto chart. Any effects that extend beyond the reference line are significant at the default level of 0.02 to 98 pct of statistical significance. The standardized mean effect expresses the mean difference between two groups in standard deviation units. In Figure 13, the only statistically significant effect on size changes after induction hardening is from the drawing angle at the beginning of the manufacturing. Combinations with the stress relief (D) and/or the P.S. angle are not significant for the statistical significance level considered; however, they cannot be disregarded and the charts can be seen as an information about their relative importance.

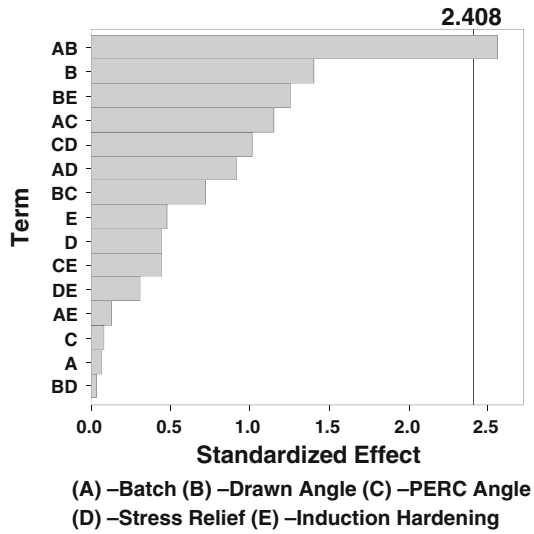

Fig. 13—Pareto charts of second-order interactions (98 pct significance level).

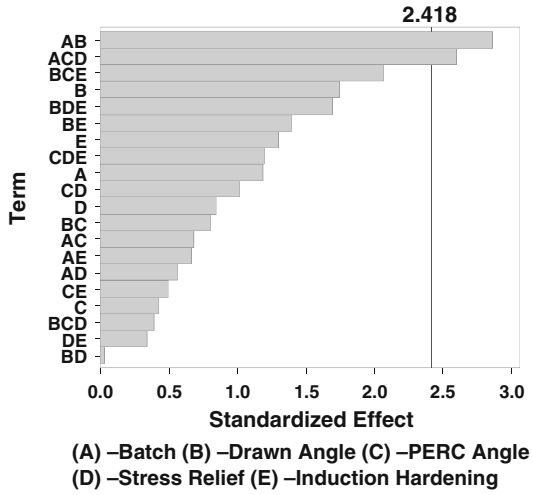

Fig. 14—Pareto charts of third-order interactions right from size change data after induction hardening (98 pct significance level). This is third-order interaction.

Figure 14 again demonstrates a consistent dependence of distortion from one single parameter: the drawing angle. Independently, if first-, second-, or third-order interactions were analyzed, the drawing angle only gives the individually required level of significance.

V. DISCUSSION

The systems approach to distortion engineering depending on investigated parameters of a multi-step manufacturing process today is an accepted but challenging procedure.[1,2,5,7,8] In a systems approach, as far as possible carriers of distortion potential should be identified as there are geometry, chemical composition, microstructure, mechanical history, temperature, and residual stresses. A DoE analysis (see Figure 4(a)) therefore of a combined cold drawing process was able to identify significant effects in a manufacturing process from cold drawing to induction hardening. Cold drawing significantly changes materials' properties of hot-rolled bars, and cold-formed automotive parts need a surface heat treatment or have to be through hardened completely to fulfill strength requirements. Normally accepted as improvement of properties during one manufacturing step can consequently result in problems in the next, one of the following, or in the last manufacturing step. Few attempts are made to optimize engineering products over more than one production step due to acquisition and distribution of semi-finished or ready products in a world market. It is well known that distortion potentials can be transmitted not only to the following but also to any of the following manufacturing steps.[2] From this investigation, it is obvious that a combined cold drawing process transmits distortion potentials from the cold drawing to the end of manufacturing—the surface hardening (see Figures 11, 12, 13, and 14). Manufacturing of these components in different companies consequently cannot be seen to be independent.

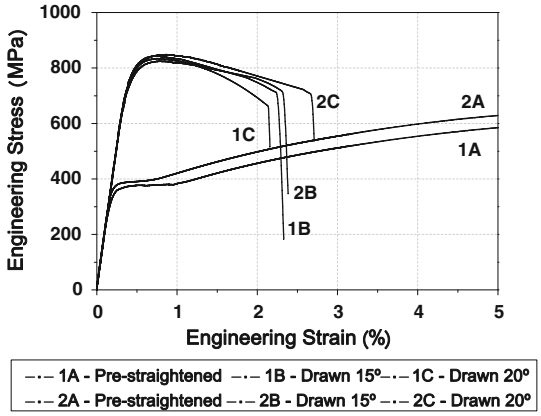

Fig. 15—Tensile test behavior of hot-rolled and pre-straightened bars from two different batches as well as stress strain curves after drawing, 1A-1B-1C batch 1, 2A-2B-2C batch 2.

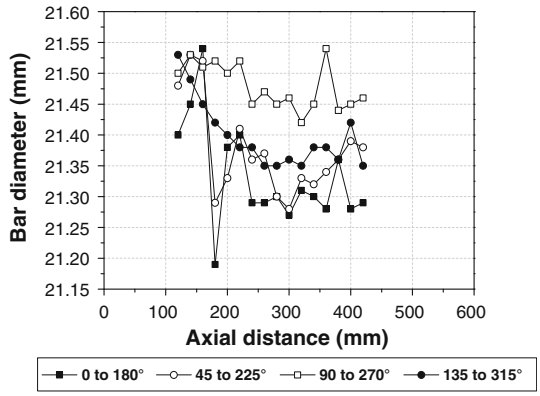

Fig. 16—Geometrical variations of pre-straightened material for selected diameters.

In this investigation, it is accepted that chemical compositions and microstructures indispensably are connected to solidified and hot-rolled bars (Figure 1). Different batches will differ to some extent and result in different stress strain curves as demonstrated in Figure 15 for tensile test samples of hot-rolled and straightened bars. The two batches for a wide range of plastic deformation show a 50 MPa load stress difference. An effect from the pre-straightening cannot be detected here because 5-mm gage diameter samples were taken from the center of pre-straightened bar, and plastic deformation during straightening is concentrated near surface layers. As Figure 6 proved, a bending state of residual stresses exists in cross sections of pre-straightened bars. In addition to the differences presented in Figure 6, Figures 15 and 16 show another problem connected to the mechanical history ahead of drawing geometry variations of hot-rolled bars. The as-delivered pre-straightened material is not circular and has locally strong diameter differences in the axial and radial direction. Additionally, the hot-rolled bar is not perfectly concentric at the die entrance cone. Unless the feeding of the hot-rolled bar in the experiments is precisely controlled, the hot-rolled bar could contact the

Table IV. Differences of Deflection (μm) After Different Manufacturing Steps (1 deg Column), Differences of Residual Stresses (MPa) After Mean Over 5-mm-Deep Surface Layer From Measurements in Figures 6, 7, 8, and 9(b) (2 deg Column), Calculation of Mean Distortion of the Samples From a Linear Fit of Residual Stress Differences (3 deg Column)

	ΔMax–Min (μm)	ΔRS Surface (MPa)	Only Bending State (MPa)
Shot Blasting	—	94	16
Drawn 15 deg	90	49	28
Drawn 20 deg	84	232	185
Drawn 15 deg-P.S. 16 deg	9	27	66
Drawn 20 deg-P.S. 16 deg	15	7	16

die at a particular periphery angle first. Besides radial diameter variations, such a condition could lead to a local variation in mechanical properties and not symmetric residual stress states after drawing.

So far it is proved that in a realistic consideration of the drawing process itself and far beyond axial-symmetric FEM modeling with perfect circular bars, it cannot be excluded at this point that geometrical, residual stress, and strain hardening variations in axial direction will have an impact on the distortion potential after drawing. Scatter is present as plotted in Figures 11 and 12, and mean deflections of all individual samples give almost similar values, *e.g.*, mean deflection is 90 μm for the 15 deg drawing and 84 μm for the 20 deg drawing angle. It should be kept in mind that the samples' lengths were 200 mm and it is clear that over a bar length of 6000 mm this deflection will not be accepted by automotive parts manufacturers. Figure 7 by local hardness measurements and Figure 14 by a macroscopic test additionally proved that drawn bars are not homogeneous as strength differences between batches and drawing angles occur after drawing and hardness show variations along different bar diameters and consequently around the periphery of analyzed bars. As expected, consequently, drawn bars show residual stress differences if one diameter line is considered and measured by Neutron diffraction analysis. Results pictures in this publication have been symmetrized to show axial and hoop stress equilibrium. If means of these stress differences are taken for the first 5 mm (0 to 5 mm) of distance from surface and compared to means of distances 15 to 20 mm, the differences in Table IV column 2 are found. Drawn bars therefore are characterized also by a bending state of residual stresses leading to a deflection as indicated in column 3 of Table IV. The two values of 28- and 185-μm deflection for drawn 15 deg and drawn 20 deg, respectively, cannot explain alone the measured distortion similar to the 2 drawing variants, as effects from other distortion potentials, components' geometry; chemical composition and local variations; mechanical history of the components; local time–temperature sequences during manufacturing; microstructure and phase transformations at temperature; and the generation and relaxation of stresses/residual stresses affect the deflection as discussed already.

It is again obvious that an additional straightening and polishing done for a straight product with precisely defined dimensions and smooth surfaces reduces the scatter in the deflection (see Table IV) as well as the

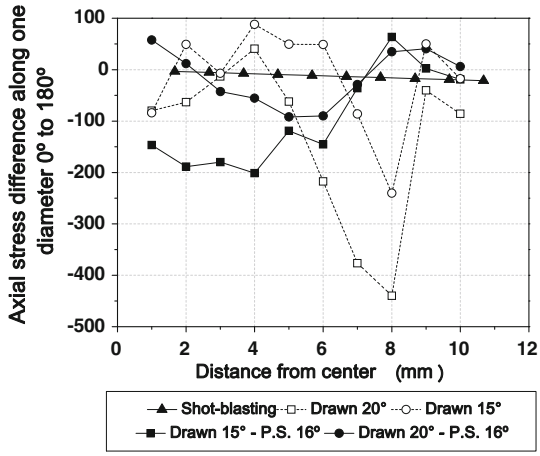

Fig. 17—Residual stress differences from a diameter line 0 to 180 deg as after neutron diffraction measurements plotted against the distances from 0 deg to the center of the bars.

residual stress differences along one diametrical line and also minimizes the high tensile residual stress from drawing (see Figure 8(b)).

From Figures 11 and 12, it is clear that stress relief treatments can separate effects of residual stresses from other distortion potentials. Reduced scatter of bar sizes can be observed (see Figure 11). From the previous discussion, a higher effect of the stress relief cannot be expected due to the influence of the other distortion potential carrier microstructure and mechanical history.

Finally, induction hardening is responsible for an increase of distortion due to time- and temperature-dependent phase transformations and the development of elastic, plastic, and transformation strains as well as transformation-induced plasticity.[19]

In spite of all additional sequences during manufacturing, the polishing and straightening, the stress relief, and the induction hardening, the highest effect on distortion results from the drawing itself as the statistical analysis of the DoE reveals (see Figures 13 and 14). The measurements of size and shape lead to the same result. Any further second-order combination from the further manufacturing does not give a statistically significant effect on distortion of size and shape. Shape changes and the calculation of distortion vectors result in a higher amount of scatter (see Figure 14). Different batches of bars from different productions sites or from different times ahead of drawing are neither homogeneous circular nor free of residual stresses. In the case,

the second-order analysis gives a statistically significant effect of batches and drawing process. Obviously, after drawing, there is also a bending state of residual stresses present and it is the question if this state of residual stresses was transferred from the pre-straightening or will be induced during the drawing process as additionally proven in Figure 17. Figure 17 displays maximum differences of residual stresses occurring in cross sections after the different manufacturing steps. These differences in residual stresses may contribute to the high amount of distortion of the bars especially after the drawing step.

VI. CONCLUSIONS

A DoE plan with main affecting parameters as pre-straightening, cold drawing, polishing/straightening, stress relief, and induction hardening was used to identify effects and correlations in a distortion analysis. A combined cold drawing process transmits parts of the distortion potentials to the following manufacturing steps. Manufacturing of these components in different companies cannot be seen to be independent. In the present case, the highest effect on distortion of drawn bars resulted from the drawing process itself. Pre-straightened material is not circular and has locally strong dimensional differences in the axial and radial direction as well as an inhomogeneous residual stress state which probably contributes to distortion after drawing. Minimizing residual stresses after cold drawing, straightening, and polishing by a stress relief treatment reduced the mean distortion level of the analyzed collection of samples and the scatter as well. On the other hand, high scatter after induction hardening can be reduced by a stress relief treatment after drawing to homogenize residual stress states. A higher induction surface hardening depth is responsible for an increase of distortion of the analyzed cylinders.

ACKNOWLEDGMENTS

This work was developed in the frame of the "BRAGECRIM" program (Brazilian German Cooperation Research Initiative in Manufacturing). The authors are deeply indebted to the DFG, CAPES, CNPq, and Finep for financial support and to HZB Berlin (neutron diffraction measurements). Preliminary cooperation also would not have been possible without support from the DAAD and CAPES. The neutron diffraction analysis has been supported by the European Commission under the 7th Framework Program through the Key Action: Strengthening the European Research Area, Research Infrastructures: Contract No. 226507 (NIMI3).

NOMENCLATURE

AISI	American Iron and Steel Institute
d_0	Interplanar spacing
DoE	Design of experiments
IH	Induction hardening
PAG	Polyalkylene glycol
P.S.	Polishing and straightening process
r	Radius
RS	Residual stress
SR	Stress relief
XRD	X-ray diffraction
SHD	Surface hardening depth
α	Statistical significance
α^1	Semi-die angle in wire drawing process

REFERENCES

1. F. Hoffmann, O. Kessler, T. Lubben, and P. Mayr: *Heat Treat. Met.*, 2004, vol. 31, pp. 27–30.
2. H.W. Zoch: *Materialwiss Werkst*, 2012, vol. 43, pp. 9–15.
3. K.D. Thoben, D. Klein, M. Seifert, and T. Wuest: *Materialwiss Werkst*, 2012, vol. 43, pp. 178–85.
4. H.L. Yu, J.W. Kang, and T.Y. Huang: *Sci. China Technol. Sci.*, 2011, vol. 54, pp. 81–87.
5. H.W. Zoch: *Materialwiss Werkst*, 2006, vol. 37, pp. 6–10.
6. T. Kuboki, H. Yoshikawa, Y. Neishi, K. Kuroda, and M. Akiyama: *Ironmak. Steelmak.*, 2001, vol. 28, pp. 117–21.
7. A.S. Rocha, R.M. Nunes, and T. Hirsch: *Proc. Inst. Mech. Eng. B*, 2012, vol. 226, pp. 459–65.
8. H. Surm, O. Kessler, F. Hoffmann, and P. Mayr: *Int. J. Mater. Prod. Technol.*, 2005, vol. 24, pp. 270–81.
9. F. Frerichs, D. Landek, T. Lubben, F. Hoffmann, and H.W. Zoch: *Materialwiss Werkst*, 2006, vol. 37, pp. 63–68.
10. J. Epp, T. Hirsch, M. Hunkel, and R. Wimpory: *Mater. Sci. Forum*, 2010, vol. 652, pp. 37–43.
11. J.M. Atienza and M. Elices: *Mater. Struct.*, 2004, vol. 37, pp. 301–04.
12. J.M. Atienza and M. Elices: *Mater. Struct.*, 2003, vol. 36, pp. 548–52.
13. M.L. Martinez-Perez, F.J. Mompean, J. Ruiz-Hervias, C.R. Borlado, J.M. Atienza, M. Garcia-Hernandez, M. Elices, J. Gil-Sevillano, R.L. Peng, and T. Buslaps: *Acta Mater.*, 2004, vol. 52, pp. 5303–13.
14. K. Tanaka and Y. Akiniwa: *JSME Int. J.*, 2004, vol. 47, pp. 252–63.
15. T. Poeste, R.C. Wimpory, and R. Schneider: *Mater. Sci. Forum*, 2006, vol. 524–525, pp. 223–28.
16. M.R. Ripoll, S.M. Weygand, and H. Riedel: *Mater. Sci. Eng. A Struct.*, 2010, vol. 527, pp. 3064–72.
17. M. Moore and W. Evans: *SAE Tech. Pap.*, 1958, vol. 66, pp. 340–45.
18. J. Epp and T. Hirsch: *Materialwiss Werkst*, 2012, vol. 43, pp. 112–19.
19. J. Epp, H. Surm, J. Kovac, T. Hirsch, and F. Hoffmann: *Metall. Mater. Trans. A*, 2011, vol. 42A, pp. 1205–14.